Synthesis and Preclinical Evaluation of a ^{68}Ga-Labeled Adnectin, ^{68}Ga-BMS-986192, as a PET Agent for Imaging PD-L1 Expression

Stephanie Robu[1], Antonia Richter*[1], Dario Gosmann*[2], Christof Seidl[1], David Leung[3], Wendy Hayes[3], Daniel Cohen[3], Paul Morin[3], David J. Donnelly[3], Daša Lipovšek[3], Samuel J. Bonacorsi[3], Adam Smith[3], Katja Steiger[4,5], Christina Aulehner[2] Angela M. Krackhardt[2,5], Wolfgang A. Weber[1,5,6]

[1]Department of Nuclear Medicine, Klinikum rechts der Isar, Technical University of Munich, Munich, Germany; [2]School of Medicine, Clinic and Policlinic for Internal Medicine III, Klinikum rechts der Isar, Technical University of Munich, Munich, Germany; [3]Bristol-Myers Squibb Research and Development, Princeton, New Jersey; [4]Institute of Pathology, School of Medicine, Technical University of Munich, Munich, Germany; [5]German Cancer Consortium, Munich, Germany, and German Cancer Research Center, Heidelberg, Germany; and [6]TranslaTUM (Zentralinstitut für translationale Krebsforschung der Technischen Universität München), Munich, Germany

Blocking the interaction of the immune checkpoint molecule programmed cell death protein-1 and its ligand, PD-L1, using specific antibodies has been a major breakthrough for immune oncology. Whole-body PD-L1 expression PET imaging may potentially allow for a better prediction of response to programmed cell death protein-1–targeted therapies. Imaging of PD-L1 expression is feasible by PET with the adnectin protein ^{18}F-BMS-986192. However, radiofluorination of proteins such as BMS-986192 remains complex and labeling yields are low. The goal of this study was therefore the development and preclinical evaluation of a ^{68}Ga-labeled adnectin protein (^{68}Ga-BMS-986192) to facilitate clinical trials. **Methods:** ^{68}Ga labeling of DOTA-conjugated adnectin (BXA-206362) was performed in NaOAc-buffer at pH 5.5 (50°C, 15 min). In vitro stability in human serum at 37°C was analyzed using radio-thin layer chromatography and radio-high-performance liquid chromatography. PD-L1 binding assays were performed using the transduced PD-L1–expressing lymphoma cell line U-698-M and wild-type U-698-M cells as a negative control. Immunohistochemical staining studies, biodistribution studies, and small-animal PET studies of ^{68}Ga-BMS-986192 were performed using PD-L1–positive and PD-L1–negative U-698-M–bearing NSG mice. **Results:** ^{68}Ga-BMS-986192 was obtained with quantitative radiochemical yields of more than 97% and with high radiochemical purity. In vitro stability in human serum was at least 95% after 4 h of incubation. High and specific binding of ^{68}Ga-BMS-986192 to human PD-L1–expressing cancer cells was confirmed, which closely correlates with the respective PD-L1 expression level determined by flow cytometry and immunohistochemistry staining. In vivo, ^{68}Ga-BMS-986192 uptake was high at 1 h after injection in PD-L1–positive tumors (9.0 ± 2.1 percentage injected dose [%ID]/g) and kidneys (56.9 ± 9.2 %ID/g), with negligible uptake in other tissues. PD-L1–negative tumors demonstrated only background uptake of radioactivity (0.6 ± 0.1 %ID/g). Coinjection of an excess of unlabeled adnectin reduced tumor uptake of PD-L1 by more than 80%. **Conclusion:** ^{68}Ga-BMS-986192 enables easy radiosynthesis and shows excellent in vitro and in vivo PD-L1–targeting characteristics. The high tumor uptake combined with low background accumulation at early imaging time points demonstrates the feasibility of ^{68}Ga-BMS-986192 for imaging of PD-L1 expression in tumors and is encouraging for further clinical applications of PD-L1 ligands.

Key Words: PD-1/PD-L1 checkpoint inhibitors; PD-L1 PET imaging; ^{68}Ga-adnectin; ^{68}Ga-BMS-986192; ^{18}F-BMS-986192

J Nucl Med 2021; 62:1228–1234
DOI: 10.2967/jnumed.120.258384

The immune system is in principle capable of recognizing and destroying cancer cells even in the presence of larger tumor masses and multiple metastases (1). However, cells of the innate and adaptive immune systems are frequently inhibited by molecular pathways that suppress their activation and effector functions and allow tumor cells to escape immune recognition and attack (2). One major checkpoint that is exploited by cancer cells to evade the immune system is the programmed death protein-1 (PD-1) pathway. The negative costimulatory receptor PD-1 is expressed on the surface of activated T cells (3,4). Its ligand, the programmed death protein ligand-1 (PD-L1), a surface protein, is expressed on both antigen-presenting cells and tumor cells of a variety of human cancers (5–7). PD-1/PD-L1 interaction induces downregulation of T-cell activation and allows tumor cells to evade immune recognition and elimination (8).

Inhibition of the PD-1/PD-L1 interaction by antibodies has been a breakthrough for the treatment of several common malignancies such as melanoma, non–small cell lung cancer, renal cell carcinoma, and urothelial cancer (9–12). However, only a subgroup of patients responds to this immune checkpoint inhibitor treatment, and the underlying reasons are not well understood (13–16). Several studies demonstrated that response to PD-1/PD-L1–targeted immunotherapy correlates with PD-L1 expression levels on tumor tissue of diverse malignancies as determined by immunohistochemistry (17). However, the quantitative analysis of PD-L1 expression in tumor tissue is challenging because of the heterogeneous and dynamic expression of such immune checkpoint molecules (18–21). Prediction of response to PD-1–targeted therapy by immunohistochemistry is therefore limited, and in several tumor types, patients benefit from PD-1–targeted therapies in the absence of significant PD-L1 expression in the tumor tissue (17,22,23).

Received Oct. 12, 2020; revision accepted Jan. 3, 2021.
For correspondence or reprints, contact Stephanie Robu (stephanie.robu@tum.de).
*Contributed equally to this work.
Published online January 30, 2021.

Imaging of PD-L1 expression can overcome several of the fundamental limitations of PD-L1 immunohistochemistry. First, imaging can provide a 3-dimensional measure of the overall PD-L1 expression of a tumor, whereas only a very small fraction of the tumor tissues can be routinely studied by immunohistochemistry. Second, imaging can assess PD-L1 expression at the whole-body level and therefore allows for studies of the heterogeneity of PD-L1 expression across multiple metastases in an individual patient. Third, imaging is noninvasive and therefore not only can provide information on PD-L1 status before the start of PD-L1 treatment but also monitor changes in PD-L1 expression at multiple times during treatment. Thus, PD-L1 imaging enables new approaches for studying PD1/PD-L1 pathophysiology in patients and may potentially allow for a better prediction of response to PD-1–targeted therapies than immunohistochemistry (24).

It is feasible to image and quantify PD-L1 expression within the tumor in patients with radiolabeled antibodies (25,26). However, antibody-based imaging has several disadvantages such as the long circulatory half-life of antibodies and their slow penetration in the tumor tissue, which necessitates imaging several days after injection. This requires the use of long-lived radioisotopes for radiolabeling, which cause the radiation exposure of antibody PET to be severalfold higher than that of PET with ^{18}F-FDG.

Adnectins are a family of engineered, target-binding proteins with a size of about 10 kDa, derived from the tenth type III domain of human fibronectin (27). Donnelly et al. synthesized and evaluated an ^{18}F-labeled anti-PD-L1 adnectin (^{18}F-BMS-986192) for PET imaging of the PD-L1 expression in vivo (28). ^{18}F-BMS-986192 showed high in vivo stability and excellent anti-PD-L1–targeting characteristics combined with fast renal clearance, resulting in high-contrast imaging of PD-L1–positive lesions up to hours after injection (28). A first-in-humans study with ^{18}F-BMS-986192 in advanced non–small cell lung carcinoma demonstrated a correlation of ^{18}F-adnectin tumor uptake with PD-L1 expression confirmed by immunohistochemistry and response to nivolumab treatment on a lesional basis. The authors illustrated that ^{18}F-BMS-986192 SUV_{peak} was higher for responding lesions than nonresponding, indicating a correlation of ^{18}F-BMS-986192 PD-L1 PET signal with PD-L1 expression and tumor-level response (29).

However, the multistep synthesis of ^{18}F-BMS-986192 with only moderate radiochemical yields is challenging and time-consuming (28,30). To facilitate a broader clinical application of anti-PD-L1 PET imaging, the development of a corresponding ^{68}Ga-labeled analog based on the adnectin scaffold seemed the conclusive next step, because of the commercial availability of Food and Drug Administration–approved ^{68}Ga/^{68}Ga-generators, the possibility of large-scale cyclotron production of ^{68}Ga, and the fast and robust ^{68}Ga-labeling technique. Herein, we report the synthesis and preclinical evaluation of ^{68}Ga-BMS-986192 in terms of PD-L1-affinity, metabolic stability, micro-PET imaging, and in vivo biodistribution in PD-L1–positive and PD-L1–negative xenografts to investigate the feasibility of this tracer for in vivo imaging of PD-L1 expression in tumors.

MATERIALS AND METHODS

Materials

All reagents were obtained from Sigma Aldrich unless otherwise stated. The DOTA-conjugated antihPD-L1 adnectin (BXA-206362) was kindly provided by Bristol-Myers-Squibb Pharmaceutical Research Institute, formulated in phosphate-buffered saline (PBS) buffer (0.9 mg/mL, pH 7.4), and tested to be endotoxin-free (1.5 EU/mg). ^{68}Ga was obtained from a ^{68}Ge/^{68}Ga generator (Galliapharm; Eckert and Ziegler AG).

Synthesis of ^{68}Ga-BMS-986192 and Quality Control

The generator was eluted in 1-mL fractions with 0.05 M aqueous HCl (4 mL) containing 170–250 MBq of $^{68}GaCl_3$. To this eluate, 1 M NaOAc (100 μL, pH 5.5) and 200 μg of DOTA-adnectin (222 μL in PBS) were added, resulting in a labeling solution at pH 5.5. The solution was mixed briefly and incubated for 15 min at 50°C. ^{68}Ga-BMS-986192 was purified by gel filtration on a PD-10 column (GE Healthcare). Radiochemical yield and radiochemical purity was analyzed by radio-thin-layer chromatography (radio-TLC) and radio-high-performance liquid chromatography. Radio-TLC was performed using Varian silica impregnated instant TLC paper (Varian Inc.) and 0.1 M aqueous sodium citrate buffer (pH 5.5) as the mobile phase. TLC strips were analyzed on a B-FC-3600 TLC Scanner (Bioscan). Analytic radio-size-exclusion chromatography of ^{68}Ga-BMS-986192 was performed using a bioZen SEC-2 (300 × 4.6 mm) column (Phenomenex LTD.) on a Shimadzu high-performance liquid chromatography system (0.1 M phosphate buffer; pH 6.8; flow, 0.35 mL/min) equipped with a NaI(TI) scintillation detector (5 × 5 cm [2 × 2 in]) and a SPD M20A diode array ultraviolet/visible-light detector.

In Vitro Stability of ^{68}Ga-BMS-986192 in Human Serum

An in vitro stability study was performed by adding ^{68}Ga-BMS-986192 (~18 MBq to freshly prepared human serum (1/8, v/v; Seronorm Human; IGZ Instruments AG), followed by incubation at 37°C for up to 4 h. To investigate the stability of ^{68}Ga-BMS-986192 in human serum, radio-high-performance liquid chromatography and radio-TLC were performed at 0, 1, 2, 3, and 4 h.

Cell Culture

The PD-L1–negative B-cell lymphoma cell line U-698-M was purchased from ATCC. Cultures were maintained in RPMI medium supplemented with 10% fetal bovine serum and penicillin/streptomycin (100 IU/mL). Cells were grown at 37°C in a humidified atmosphere of 5% CO_2. To stably express PD-L1, the U-698-M cells were retrovirally transduced with a construct containing genes for human PD-L1 and green fluorescent protein, as previously described (31). Quantification of PD-L1 expression on transduced and wild-type U-698-M cells was determined by fluorescence-activated cell sorting (FACS) analysis using an antihuman CD274 antibody (Clone MIH1; BD Bioscience) as previously described (32).

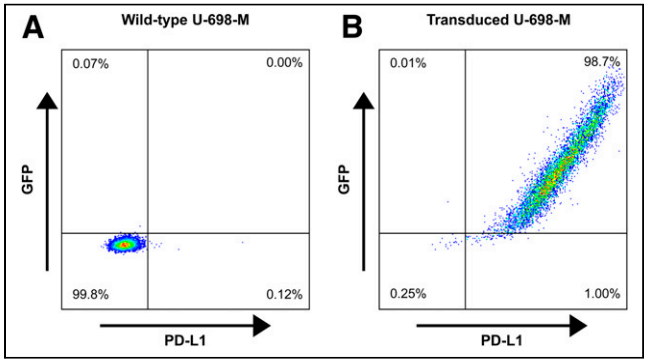

FIGURE 1. Representative dot-plots of expression of green fluorescent protein and PD-L1 in wild-type U-698-M cells (A) and in U-698-M cells transduced by retroviral vector MP71 containing PD-L1 and green fluorescent protein (GFP) separated by P2A element (B).

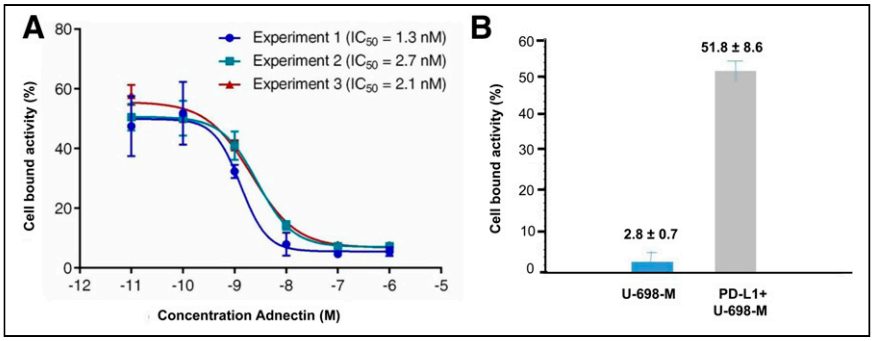

FIGURE 2. Binding affinity and specificity of ^{68}Ga-BMS-986192 toward PD-L1 in competitive radioligand binding assays. (A) Cell-bound activity in presence of increasing concentrations of cold ligand (BXA-206362). (B) Cell-bound activity in presence of cold ligand (0.1 nM) on PD-L1–positive (gray bar) and PD-L1–negative (blue bar) U-698-M cells. IC_{50} = half-maximal inhibitory concentration.

Assessment of PD-L1 Binding Affinity and Specificity

The binding affinity of ^{68}Ga-BMS-986192 toward human PD-L1 was determined in a competitive binding experiment using stable transduced U-698-M PD-L1 cells with elevated PD-L1 expression. Briefly, a solution containing a mixture of ^{68}Ga-labeled (25 μL) and unlabeled DOTA-conjugated antihPD-L1 adnectin (25 μL, competitor) with increasing concentrations (10^{-10}–10^{-6} M) was added to the cells (400,000 cells per vial). After 1 h of incubation at 37°C, the cells were centrifuged at 600*g* (1,200 rpm; Biofuge 15) for 5 min, the supernatant of each vial was removed, and the cells were thoroughly washed 2 times with 250 μL of PBS. The washing medium was combined with the previously removed supernatant, representing the amount of free radioligand. The amount of cell-bound activity (cell pellet), as well as the amount of free radioligand, was measured in a 2470 Wizard^2 γ-counter (PerkinElmer). Because of the high structural similarity of ^{68}Ga-labeled and unlabeled ligand, a nearly identical affinity for PD-L1 is assumed, resulting in homologous competitive binding. Specific binding was confirmed using nontransduced U-689-M cells as a negative control.

U-698-M Tumor Model

All animal experiments were conducted according to the current animal welfare regulations in Germany (DeutschesTierschutzgesetz, approval ROB-55.2–2532.-Vet_02–15–216). The transduced U-698-M PD-L1–positive and U-698-M wild-type cell lines were detached from the surface of the culture flask using trypsin/ethylenediaminetetraacetic acid (0.05% and 0.02%) in PBS, centrifuged, and resuspended in PBS. Approximately 1×10^7 cells/200 μL of the U-698-M PD-L1–positive cell line were inoculated subcutaneously on the right flank, and U-698-M wild-type cells on the left flank, of 6- to 8-wk-old male NSG mice (Charles River WIGA GmbH). Tumors were grown for 2–3 wk to reach 0.6–1 cm in diameter.

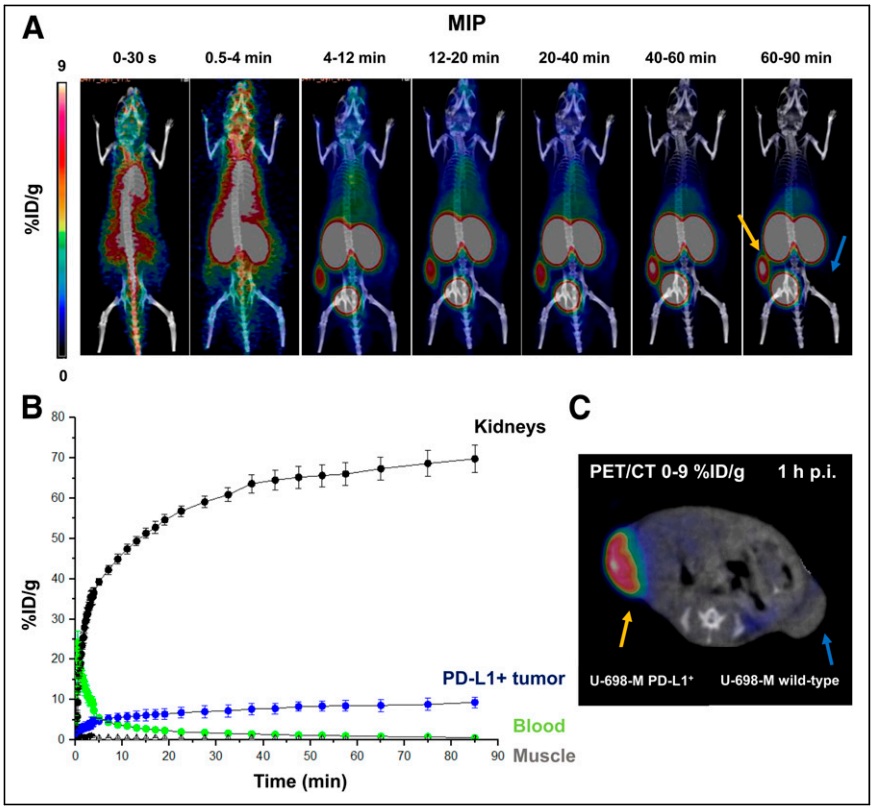

FIGURE 3. Dynamic ^{68}Ga-BMS-986192 PET/CT imaging in anesthetized PD-L1–positive and wild-type U-698-M xenograft–bearing NSG mice. (A) Summation maximum-intensity projections (MIP) of different time frames during 90-min acquisition. (B) Time–activity curves for blood pool (heart), kidneys, muscle, and PD-L1–positive tumor derived from dynamic data. (C) Axial PET/CT scan at 1 h after injection (p.i.).

Small-Animal PET Imaging

The mice were anesthetized with isoflurane and intravenously injected via the tail vein with approximately 5–7 MBq (~4.5–5.5 μg) of ^{68}Ga-BMS-986192. In vivo imaging studies were performed using a Siemens Inveon small-animal PET/CT scanner. Static images were recorded at 1 h and 2 h after injection with an acquisition time of 20 min. For blocking studies, unlabeled BXA-206362 (9 mg/kg) was coinjected with ^{68}Ga-BMS-986192. Dynamic imaging was performed after on-bed injection for 1.5 h under isoflurane anesthesia. Reconstruction of the images was performed using a 3-dimensional ordered-subsets expectation maximum algorithm with scanner and attenuation correction. Data analysis was performed using Inveon Workplace software (Siemens). Regions of interest were drawn around areas with increased uptake in transaxial slices for calculation of the average tracer concentration as percentage injected dose (%ID)/g.

Ex Vivo Histology and Immunohistochemistry

Tumor tissues were fixed in 10% neutral-buffered formalin solution for at least 48 h, dehydrated under standard conditions (Leica ASP300S), and embedded in paraffin. Serial 2-μm-thick sections prepared with a rotary microtome (HM355S; Thermo Fisher Scientific) were collected and subjected to histologic and immunohistochemical analysis. Hematoxylin–eosin staining was performed on deparaffinized sections with eosin and

Mayer hematoxylin according to a standard protocol.

Immunohistochemistry was performed using a Bond RXm system (Leica) with primary antibodies against human PD-L1 (clone 28–8, ab205921, 1:500).

Ex Vivo Biodistribution

About 5–7 MBq of ^{68}Ga-BMS-986192 (4.5–5.5 μg) were injected into the tail vein of the U-698-M-PD-L1–positive and U-698-M wild-type tumor–bearing NSG mice under isoflurane anesthesia. The animals were sacrificed at 1 h after injection ($n = 4$) or 2 h after injection ($n = 4$), the organs of interest were dissected, and the activity in the weighed tissues samples was quantified using a γ-counter.

RESULTS

^{68}Ga Labeling and In Vitro Stability of ^{68}Ga-BMS-986192 in Human Serum

High labeling efficiencies with quantitative radiochemical yields of more than 97% were obtained after 15 min. After purification, moderate specific activities of 11–16 GBq/μmol and radiochemical purity of more than 98% was achieved.

Radio-high-performance liquid chromatography of ^{68}Ga-BMS-986192 at various time points after mixing with human serum revealed monomeric elution profiles with a minimal radioactive impurity of higher molecular weight (8.97 min), which slightly increased up to 5% after 4 h. Radio-TLC analysis revealed moderate transmetallation (5%) for ^{68}Ga-BMS-986192 within 4 h (Supplemental Fig. 1; supplemental materials are available at http://jnm.snmjournals.org).

Characterization of PD-L1 Expression in Transduced U-698-M Cells

Quantification of PD-L1 expression on transduced and wild-type U-698-M cells was determined by FACS analysis. A low PD-L1 expression of approximately 4,000 molecules per cell was observed for wild-type U-698-M cells (Fig. 1). PD-L1 expression was significantly increased by stable transduction of U-698-M cells, with approximately 155,000 PD-L1 molecules per cell.

Competitive Binding Assay of ^{68}Ga-BMS-986192 to PD-L1

Binding affinity of ^{68}Ga-BMS-986192 to human PD-L1 was determined in a competitive radioligand binding experiment using PD-L1–positive and wild-type U-698-M cells. ^{68}Ga-BMS-986192 showed high affinity toward human PD-L1 with a half-maximal inhibitory concentration of 2.0 ± 0.6 nM (Fig. 2A). Specific binding was confirmed using nontransduced U-698-M cells as a negative control (Fig. 2B).

PET/CT Imaging

^{68}Ga-BMS-986192 showed a rapid clearance from the blood pool and from nontarget tissues, with continuously increasing accumulation in the kidneys over time (Figs. 3A and 3B). ^{68}Ga-BMS-986192 uptake in PD-L1–positive tumor was fast within 4 min after injection, and tracer accumulation in PD-L1–expressing tumor tissue increased within 60 min, with high retention over 90 min after injection (Figs. 3A and 3C). No uptake in the PD-L1–negative U-698-M tumor was observed.

Additional static small-animal PET scans were performed with ^{68}Ga-BMS-986192 in PD-L1–positive and PD-L1 wild-type tumor–bearing NSG mice at 1 and 2 h after injection (Fig. 4A). ^{68}Ga-BMS-986192 showed comparably high tumor uptake in PDL-1–positive tumors after 1 and 2 h after injection. As shown in Figure 4A, in contrast to the high uptake of ^{68}Ga-BMS-986192 in PD-L1–positive U-698-M tumors, no accumulation was observed in U-698-M wild-type xenografts, confirming PD-L1 specific binding of ^{68}Ga-BMS-986192. Additionally, blocking experiments with an excess of unlabeled adnectin (9 mg/kg) demonstrated that ^{68}Ga-BMS-986192 uptake is specific and mediated by PD-L1 (Fig. 4B).

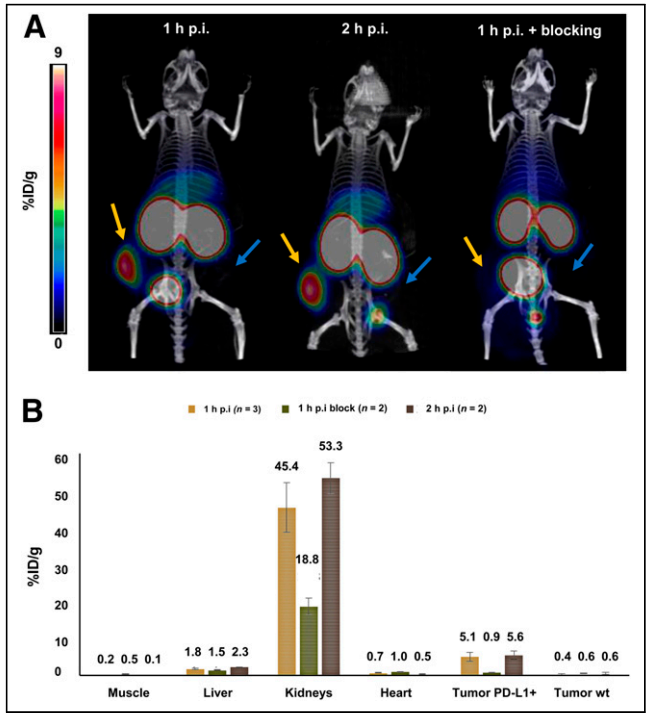

FIGURE 4. (A) Static ^{68}Ga-BMS-986192 PET imaging examples in PD-L1–positive (yellow arrows) and wild-type (blue arrows) U-698-M xenograft–bearing NSG mice. Images are maximum-intensity projections (5–6 MBq, 4.5–5.5 μg) obtained at 1 and 2 h after injection (p.i.). Mouse at far right received ^{68}Ga-BMS-986192 plus blocking with unlabeled adnectin, 9 mg/kg. (B) ROI quantification of static PET scans (mean %ID/g).

Ex Vivo FACS Analysis, Histology, and Immunohistochemistry

Ex vivo FACS analysis of dissected tumors confirmed the correlation of ^{68}Ga-BMS-986192 uptake with PD-L1 expression levels in tumor tissue (Figs. 5A and 5B). PD-L1 expression levels in transduced U-698-M tumors was highly increased in comparison to nontransduced U-698-M wild-type xenografts, confirming the generation of a stable PD-L1–expressing tumor cell line in vivo and PD-L1–mediated uptake of ^{68}Ga-BMS-986192.

Ex vivo histology and immunohistochemistry of the xenograft tissues also revealed high and homogeneous PD-L1 expression in U-698-M PD-L1–positive tumors, whereas no PD-L1 expression was found in U-698-M wild-type tissues (Fig. 5C). These results confirm the PD-L1–specific uptake of ^{68}Ga-BMS-986192 in small-animal PET imaging in vivo and correlate with ex vivo flow cytometry analysis.

Biodistribution

The biodistribution data of ^{68}Ga-BMS-986192 in PD-L1–positive-U-698-M and U-698-M wild-type tumor–bearing mice (1 and 2 h after injection) are shown in Figure 6 and Supplemental Table 1. The data reflect the results of small-animal PET/CT imaging. ^{68}Ga-BMS-986192 exhibited predominant renal clearance, with only slight uptake in the liver and nontargeted tissues. The significant uptake of ^{68}Ga-BMS-986192 in PD-L1–positive tumor

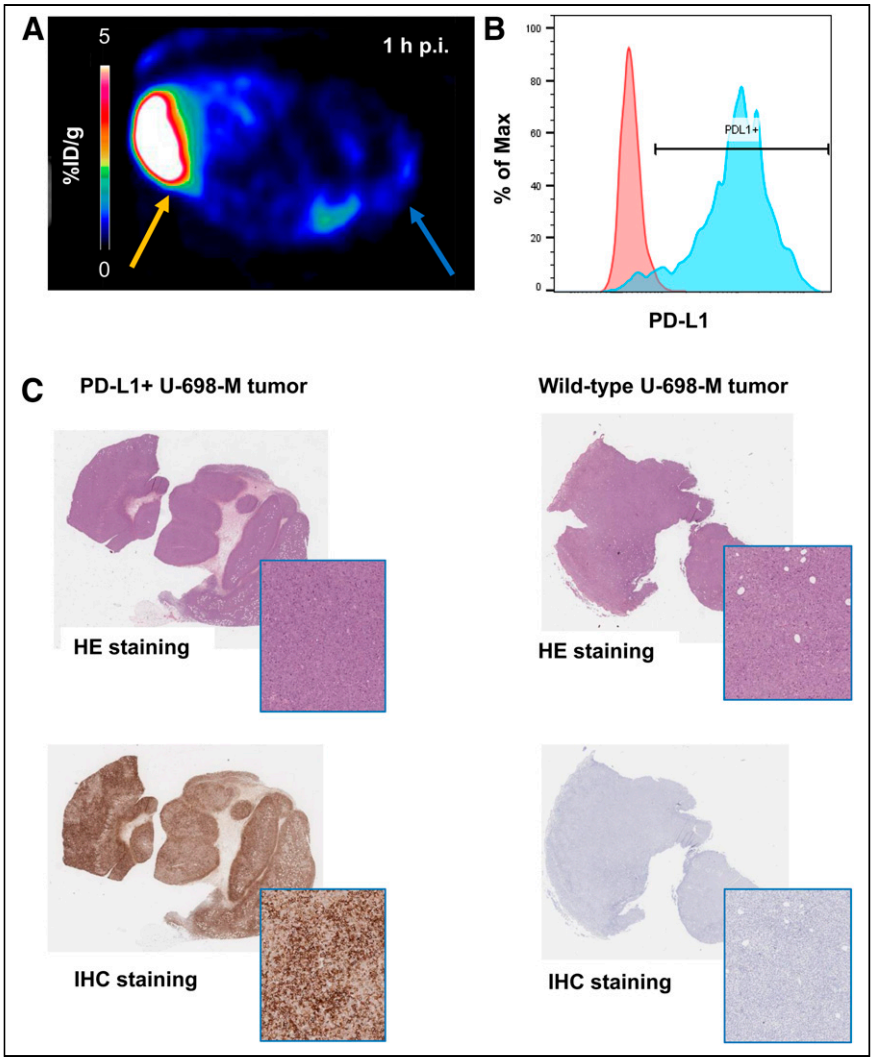

FIGURE 5. (A) Axial ^{68}Ga-BMS-986192 PET scan at 1 h after injection in PD-L1–positive (yellow arrow) and wild-type (blue arrow) U-698-M xenograft–bearing NSG mouse. (B) Ex vivo FACS analysis of PD-L1 expression on wild-type (red) and PD-L1 transduced (blue) tumor cells. (C) Ex vivo hematoxylin–eosin (HE) and anti-PD-L1 immunohistochemistry (IHC) staining of PD-L1–positive and wild-type xenograft tissues.

xenografts is highly specific, as accumulation in PD-L1–negative tumors was less than blood-pool activity (Supplemental Table 1).

DISCUSSION

This study revealed that the high-affinity PD-L1–binding adnectin protein BMS-986192, conjugated at the C terminal position with DOTA via maleimide linkage (BXA-206362), can be labeled with ^{68}Ga while retaining high target binding affinity (half-maximal inhibitory concentration, 2.0 ± 0.6 nM determined in a competitive radioligand binding assay using PD-L1–positive U-698-M cells). The DOTA-maleimide moiety was conjugated to the cysteine residue engineered into the C terminus of the adnectin (28,30). The same position within the adnectin scaffold has been used previously for site-specific conjugation of the ^{18}F-labeled prosthetic group of ^{18}F-BMS-986192 without a significant effect on binding affinity (28). ^{19}F-BMS-986192, an unmodified and DOTA-conjugated adnectin, has displayed picomolar dissociation constants against human PD-L1 determined by surface plasmon resonance (28). This indicates that conjugation of small molecules to the C terminus of adnectin is well tolerated, without observable effects on human PD-L1 binding. The ease of tracer preparation and the quantitative radiochemical yields with high radiochemical purity make the synthesis of ^{68}Ga-BMS-986192 fully compatible with the everyday workflow in a clinical radiopharmacy and are well suited for automated radiosynthesis via a module or a kit formulation. Furthermore, the pharmacokinetics of ^{68}Ga-BMS-986192 match very well the 68-min physical half-life of ^{68}Ga, as peak tumor uptake reached a plateau within 60 min after injection. Collectively, these characteristics are highly encouraging for using ^{68}Ga-BMS-986192 to image PD-L1 expression in humans.

Small-animal PET and ex vivo biodistribution studies demonstrated excellent targeting of PD-L1–expressing xenografts, whereas tracer uptake was low in tumors without PD-L1 expression on immunohistochemistry (Figs. 4 and 5). The specificity of tracer binding was further confirmed by coinjection of an excess of unlabeled BMS-986192, which decreased tumor uptake of ^{68}Ga-BMS-986192 by 80% (Fig. 6). As expected for a 10-kDa protein, ^{68}Ga-BMS-986192 showed fast renal clearance from the blood. As observed for other small proteins, peptides and peptide-like molecules, ^{68}Ga-BMS-986192 showed significant retention of activity in the kidneys at 1 and 2 h after injection. However, the activity concentration was similar to that of clinically used PET imaging agents such as prostate-specific membrane ligands (33,34). Therefore, we do not expect renal uptake of ^{68}Ga-BMS-986192 to limit its clinical use. Injection of an excess of unlabeled adnectin significantly decreased renal uptake of ^{68}Ga-BMS-986192. This is unlikely to be due to blocking of PD-L1 binding since BMS986192 has only low affinity for murine PD-L1 (28). Nevertheless, it indicates that renal uptake of radioactivity is a partially saturable process that could potentially be reduced by injection of proteins or peptides that do not interfere with the binding of ^{68}Ga-BMS-986192 to its target. The activity concentration in the kidneys increased from 1 to 2 h after injection, probably reflecting redistribution of the ligand from other tissues to the bloodstream (Fig. 6).

A comparison of the preclinical results obtained for ^{18}F-BMS986192 and ^{68}Ga-BMS-986192 revealed similar specific activities and similar in vitro and in vivo behavior for both tracers (28). Although comparable protein and activity doses of ^{18}F-BMS986192 and ^{68}Ga-BMS-986192 were administered to mice, a direct comparison of the tumor uptake of both radiolabeled ligands is not feasible as different cell lines were used in the 2 studies, but both tracers showed similar pharmacokinetics, with fast renal

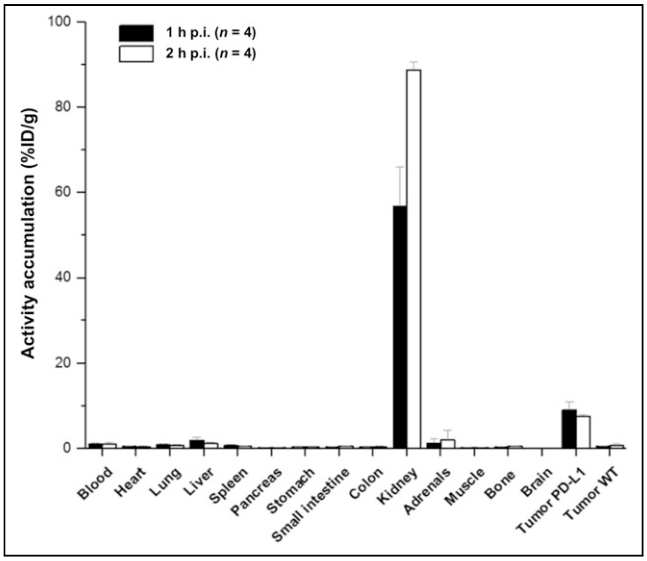

FIGURE 6. Biodistribution data for ^{68}Ga-BMS-986192 in PD-L1–positive and wild-type (WT) U-698-M xenograft–bearing mice at 1 and 3 h after injection (p.i.). Data are %ID/g (mean ± SD).

clearance and similarly low background activity in all other organs. This is encouraging for the clinical translation of ^{68}Ga-BMS-986192 because PET imaging of PD-L1 expression with ^{18}F-BMS-986192 has already been shown to be feasible in human pilot studies (29,35).

The following limitation of the study should be noted. ^{68}Ga-BMS-986192 exclusively binds to human PD-L1, with no relevant affinity toward its murine counterpart (28). Tumor-to-normal organ uptake ratios may therefore be lower in humans than in our mouse model. Furthermore, we used a PD-L1 transduced cell line to study the binding of ^{68}Ga-BMS-986192. The advantages of this approach are that the parent cell line can be used as a negative control to assess the specificity of ligand binding. Furthermore, the stable expression of PD-L1 improves the reproducibility of these results to ensure having a tool for measurement PD-L1 expression of cancer cells, as endogenous cancer cell PD-L1 expression is known to vary significantly over time (36). However, PD-L1 expression levels may be higher in PD-L1 transduced U698-M cells than in human tumors.

CONCLUSION

The novel PD-L1 imaging agent ^{68}Ga-BMS-986192 shows similar PD-L1–targeting characteristics and pharmacokinetic properties to ^{18}F-BMS-986192, which has already been successfully used to image PD-L1 expression in cancer patients. In contrast to ^{18}F-BMS-986192, which requires a 2-step synthesis with low radiochemical yields, radiolabeling of BMS-986192 with ^{68}Ga is a straightforward 1-step process that is easy to automate. ^{68}Ga-BMS-986192 therefore has the potential to significantly facilitate preclinical and clinical imaging of PD-L1 expression.

DISCLOSURE

The current study was financially supported by the Deutsche Forschungsgemeinschaft (SFB824; subprojects C10, Z1, and Z2). David Leung, Wendy Hayes, Paul Morin, Adam Smith, David Donnelly, Daša Lipovšek, Sam Bonacorsi, and Daniel Cohen are employed by Bristol-Myers Squibb Co. ^{18}F-BMS-986192 and ^{68}Ga-BMS-986192 are the subject of patent applications WO2016086021A1, WO2016086036A2, WO2017/210302, and WO2017/210335. No other potential conflict of interest relevant to this article was reported.

ACKNOWLEDGMENTS

We thank Sybille Reder, Markus Mittelhäuser, and Hannes Rolbiesky for small-animal PET imaging and Olga Seelbach and Marion Mielke for hematoxylin–eosin and immunohistochemistry staining.

KEY POINTS

QUESTION: Can adnectins be efficiently radiolabeled with ^{68}Ga to allow the in vivo assessment and quantification of PD-L1 expression levels on tumor tissue with PET?

PERTINENT FINDINGS: The expansion of the adnectin-based concept for PD-L1 expression PET imaging to the requirements of ^{68}Ga chemistry enables fast and efficient radiolabeling. ^{68}Ga-BMS-986192 showed comparable in vitro and in vivo PD-L1–targeting characteristics to its counterpart, ^{18}F-BMS986192. Both tracers showed favorable pharmacokinetics, with fast renal clearance and similarly low background activity in nontargeted tissues.

IMPLICATIONS FOR PATIENT CARE: The preclinical results are encouraging for the clinical translation of ^{68}Ga-BMS-986192 because PET imaging of PD-L1 expression with ^{18}F-BMS-986192 has already been shown to be feasible in human pilot studies.

REFERENCES

1. Gonzalez H, Hagerling C, Werb Z. Roles of the immune system in cancer: from tumor initiation to metastatic progression. *Genes Dev.* 2018;32:1267–1284.
2. Topalian SL, Drake CG, Pardoll DM. Immune checkpoint blockade: a common denominator approach to cancer therapy. *Cancer Cell.* 2015;27:450–461.
3. Riella LV, Paterson AM, Sharpe AH, Chandraker A. Role of the PD-1 pathway in the immune response. *Am J Transplant.* 2012;12:2575–2587.
4. Keir ME, Butte MJ, Freeman GJ, Sharpe AH. PD-1 and its ligands in tolerance and immunity. *Annu Rev Immunol.* 2008;26:677–704.
5. Konishi J, Yamazaki K, Azuma M, Kinoshita I, Dosaka-Akita H, Nishimura M. B7-H1 expression on non-small cell lung cancer cells and its relationship with tumor-infiltrating lymphocytes and their PD-1 expression. *Clin Cancer Res.* 2004;10:5094–5100.
6. Thompson RH, Gillett MD, Cheville JC, et al. Costimulatory B7-H1 in renal cell carcinoma patients: indicator of tumor aggressiveness and potential therapeutic target. *Proc Natl Acad Sci USA.* 2004;101:17174–17179.
7. Hino R, Kabashima K, Kato Y, et al. Tumor cell expression of programmed cell death-1 ligand 1 is a prognostic factor for malignant melanoma. *Cancer.* 2010;116:1757–1766.
8. Freeman GJ, Long AJ, Iwai Y, et al. Engagement of the PD-1 immunoinhibitory receptor by a novel B7 family member leads to negative regulation of lymphocyte activation. *J Exp Med.* 2000;192:1027–1034.
9. Herbst RS, Baas P, Kim DW, et al. Pembrolizumab versus docetaxel for previously treated, PD-L1-positive, advanced non-small-cell lung cancer: a randomised controlled trial. *Lancet.* 2016;387:1540–1550.
10. Weinstock M, McDermott D. Targeting PD-1/PD-L1 in the treatment of metastatic renal cell carcinoma. *Ther Adv Urol.* 2015;7:365–377.
11. Simeone E, Ascierto PA. Anti-PD-1 and PD-L1 antibodies in metastatic melanoma. *Melanoma Manag.* 2017;4:175–178.
12. Stenehjem DD, Tran D, Nkrumah MA, Gupta S. PD1/PDL1 inhibitors for the treatment of advanced urothelial bladder cancer. *Onco Targets Ther.* 2018;11:5973–5989.
13. Alsaab HO, Sau S, Alzhrani R, et al. PD-1 and PD-L1 checkpoint signaling inhibition for cancer immunotherapy: mechanism, combinations, and clinical outcome. *Front Pharmacol.* 2017;8:561.
14. Chen L, Han X. Anti-PD-1/PD-L1 therapy of human cancer: past, present, and future. *J Clin Invest.* 2015;125:3384–3391.
15. Cottrell TR, Taube JM. PD-L1 and emerging biomarkers in immune checkpoint blockade. *Cancer J.* 2018;24:41–46.

16. Zou W, Wolchok JD, Chen L. PD-L1 (B7-H1) and PD-1 pathway blockade for cancer therapy: mechanisms, response biomarkers, and combinations. *Sci Transl Med.* 2016; 8:328rv4.
17. Chakravarti N, Prieto VG. Predictive factors of activity of anti-programmed death-1/programmed death ligand-1 drugs: immunohistochemistry analysis. *Transl Lung Cancer Res.* 2015;4:743–751.
18. Kloten V, Lampignano R, Krahn T, Schlange T. Circulating tumor cell PD-L1 expression as biomarker for therapeutic efficacy of immune checkpoint inhibition in NSCLC. *Cells.* 2019;8:809.
19. Yue C, Jiang Y, Li P, et al. Dynamic change of PD-L1 expression on circulating tumor cells in advanced solid tumor patients undergoing PD-1 blockade therapy. *OncoImmunology.* 2018;7:e1438111.
20. Madore J, Vilain RE, Menzies AM, et al. PD-L1 expression in melanoma shows marked heterogeneity within and between patients: implications for anti-PD-1/PD-L 1 clinical trials. *Pigment Cel Melanoma Res.* 2015;28:245–253.
21. Niemeijer AN, Leung D, Huisman M, et al. Whole body PD-1 and PD-L1 positron emission tomography in patients with non-small-cell lung cancer. *Nat Commun.* 2018;9:4664.
22. Ribas A, Hu-Lieskovan S. What does PD-L1 positive or negative mean? *J Exp Med.* 2016;213:2835–2840.
23. Abdel-Rahman O. Correlation between PD-L1 expression and outcome of NSCLC patients treated with anti-PD-1/PD-L1 agents: a meta-analysis. *Crit Rev Oncol Hematol.* 2016;101:75–85.
24. Broos K, Lecocq Q, Raes G, Devoogdt N, Keyaerts M, Breckpot K. Noninvasive imaging of the PD-1:PD-L1 immune checkpoint: embracing nuclear medicine for the benefit of personalized immunotherapy. *Theranostics.* 2018;8:3559–3570.
25. Heskamp S, Hobo W, Molkenboer-Kuenen JD, et al. Noninvasive imaging of tumor PD-L1 expression using radiolabeled anti-PD-L1 antibodies. *Cancer Res.* 2015;75: 2928–2936.
26. Truillet C, Oh HLJ, Yeo SP, et al. Imaging PD-L1 expression with immunoPET. *Bioconjug Chem.* 2018;29:96–103.
27. Lipovšek D. Adnectins: engineered target-binding protein therapeutics. *Protein Eng Des Sel.* 2011;24:3–9.
28. Donnelly DJ, Smith RA, Morin P, et al. Synthesis and biological evaluation of a novel ^{18}F-labeled adnectin as a PET radioligand for imaging PD-L1 expression. *J Nucl Med.* 2018;59:529–535.
29. Niemeijer AN, Leung D, Huisman MC, et al. Whole body PD-1 and PD-L1 positron emission tomography in patients with non-small-cell lung cancer. *Nat Commun.* 2018;9:4664.
30. Morin PE, Donnelly D, Lipovsek D, inventors; Bristol-Myers Squibb Company, USA, assignee. Novel PD-L1-binding polypeptides for imaging. U.S. patent WO2016086021A1. 2016.
31. Audehm S, Glaser M, Pecoraro M, et al. Key features relevant to select antigens and TCR from the MHC-mismatched repertoire to treat cancer. *Front Immunol.* 2019;10: 1485.
32. Mayer KE, Mall S, Yusufi N, et al. T-cell functionality testing is highly relevant to developing novel immuno-tracers monitoring T cells in the context of immunotherapies and revealed CD7 as an attractive target. *Theranostics.* 2018;8:6070–6087.
33. Weineisen M, Schottelius M, Simecek J, et al. ^{68}Ga-and ^{177}Lu-labeled PSMA I&T: optimization of a PSMA-targeted theranostic concept and first proof-of-concept human studies. *J Nucl Med.* 2015;56:1169–1176.
34. Robu S, Schmidt A, Eiber M, et al. Synthesis and preclinical evaluation of novel ^{18}F-labeled Glu-urea-Glu-based PSMA inhibitors for prostate cancer imaging: a comparison with ^{18}F-DCFPyl and ^{18}F-PSMA-1007. *EJNMMI Res.* 2018;8:30.
35. Huisman MC, Niemeijer AL, Windhorst B, et al. Quantification of PD-L1 expression with [^{18}F]BMS-986192 PET/CT in patients with advanced stage non-small-cell lung cancer. *J Nucl Med.* 2020;61:1455–1460.
36. Yue C, Jiang Y, Li P, et al. Dynamic change of PD-L1 expression on circulating tumor cells in advanced solid tumor patients undergoing PD-1 blockade therapy. *OncoImmunology.* 2018;7:e1438111.